

Preparation and Electrochemical Performance of Li-rich Cathode Material $\text{Li}_{1.17}[\text{Ni}_{0.17}\text{Co}_{0.17}\text{Mn}_{0.50}]\text{O}_2$ Synthesized by Solid State Method via Acetate Precursor for Li-ion Batteries

Xinnuan Liu¹, Luozeng Zhou² and Qunjie Xu^{1,*}

¹ Shanghai Key Laboratory of Materials Protection and Advanced Materials in Electric Power, College of Environmental and Chemical Engineering, Shanghai University of Electric Power, 2103 Pingliang Road, Yangpu District, Shanghai, 200090, China

² Shanghai Institute of Space Power Source(SISP), 2965 Dongchuan Road, Minghang District, Shanghai, 200245, China

*E-mail: xuqunjie@shiep.edu.cn

Received: 7 July 2015 / Accepted: 25 August 2015 / Published: 30 September 2015

The lithium rich “layered-layered” cathode material $\text{Li}_{1.17}[\text{Ni}_{0.17}\text{Co}_{0.17}\text{Mn}_{0.50}]\text{O}_2$ has been successfully synthesized via acetate precursor by solid state method. XRD and SEM characterizations illustrate a well-ordered layered structure and homogeneous primary particles, which might be greatly contributing to electrochemical performance. The initial reversible capacity of this Li-rich composite electrode could be achieved as high as 240.1 mAh g⁻¹ at 0.1C. No obvious capacity fading could be observed while cycled at different C-rates after initial capacity decay. High initial discharge capacities of 218.2 mAh g⁻¹ at 0.2C, 199.3 mAh g⁻¹ at 0.5C, 177.5 mAh g⁻¹ at 1C, 161.5 mAh g⁻¹ at 2C and 131.6 mAh g⁻¹ at 5C have been performed within the cutoff voltage limits of 2.0 V to 4.8 V at room temperature and steady reversible discharge capacity has been delivered in long-term cycles.

Keywords: Li-rich cathode material; Solid state method; Electrochemical performance

1. INTRODUCTION

Layered transition metal oxides have been investigated massively during the last three decades as cathode materials for lithium ion battery since the first introduction and commercialization of cobaltite LiCoO_2 by Sony in 1990 [1]. As LiCoO_2 suffers some defects like high cost, toxicity, and low useful capacity (only 50% to 60% of theoretical capacity could be utilized in practical application), several kinds of layered multi-transition metal oxides has been developed as promising cathode alternatives to LiCoO_2 . Notable among them are the various layered Li-Ni-Co-Mn oxide cathode

compounds intensively studied in past few years due to the significant advantages over traditional cathode materials of Li-ion battery system [2,3].

Since serious drawbacks like poor electrochemical performance on cyclic life, low energy density and safety problems inhibiting the further usage of LiCoO₂ and layered iso-structural Li-Ni-Co-Mn oxide compounds as lithium ion battery cathodes in the fields of hybrid and pure electric vehicles [4-7], recent developments of cathode alternatives for Li-ion batteries have been focusing on the "layered-layered" solid solution series between Li₂MnO₃ (or Li[Li_{1/3}Mn_{2/3}]O₂) and LiMO₂ (Where M=Ni, Co, Mn, ect...). These cathode compounds can be represented by either (i) structurally layered-layered components notation like $x\text{Li}_2\text{MnO}_3 \cdot (1-x)\text{LiMO}_2$, where the Li₂MnO₃ could be electrochemically activated above 4.4 V vs. Li/Li⁺ [6-9]; or (ii) standard notation as Li_{1+y}M_{1-y}O₂ (M=Ni, Co, Mn) [8-12]. Such Li-rich cathodes usually could deliver a very high discharge capacity approximately over 240 mAh g⁻¹ between potential cutoff ranges from 2.0 V to 4.8V. For instance, Li[Li_{0.2}Ni_{0.13}Co_{0.13}Mn_{0.54}]O₂, which is also noted as in the form of 0.6Li₂MnO₃·0.4Li[Ni_{1/3}Co_{1/3}Mn_{1/3}]O₂, has been widely investigated for its high initial capacity above 250 mAh g⁻¹ within cutoff voltage of 2.0 V to 4.8 V [13-17]. However, there are still major issues, such as the poor rate capacity, significant irreversible capacity fade in initial cycle, and discharge voltage plateau decrease upon cycling, that need to be well resolved before these Li-rich compounds could be considered as high-energy cathodes for Li-ion batteries, specifically in application for electric vehicles.

As well-known, the electrochemical performance of cathodes is extremely interrelated with morphology and particle size distribution, which would be highly affected by precursor treating process. A very narrow particle size distribution and homogeneous morphology could be expected when the cathode precursors are obtained by liquid-phase method throughout almost complete mixture for raw materials of cathode precursors at the molecular level among the liquid solvents [16-22]. Although solid state treatments for cathode precursors always generate pretty larger cathode particles with irregular morphology, the solid state method is still the most common synthesis approach for cathodes in real production by reason of easy accessibility and economic cost [23].

In this paper, we introduce a much more convenient and effective route which integrated the superiority of liquid-phase and solid state method in cathode material preparation with very excellent electrochemical performance for Li-ion batteries by acetate precursors, especially in the preparation of layered-layered Li-rich cathodes Li_{1+y}M_{1-y}O₂ (M=Ni, Co, Mn). This paper reports the synthesis and electrochemical performance of a novel Li-rich Li_{1.17}[Ni_{0.17}Co_{0.17}Mn_{0.50}]O₂ cathode prepared via acetate precursor by solid state method. The structure, morphology and electrochemical properties are set forth as following.

2. EXPERIMENTAL

Lithium rich cathode Li_{1.17}[Ni_{0.17}Co_{0.17}Mn_{0.50}]O₂ (hereafter Li-rich NCM) was prepared via the acetate precursors by solid state method of segmented calcination. Stoichiometric amount of lithium acetate (CH₃COOLi·2H₂O, 99.0%, Sinopharm), nickel acetate ((CH₃COO)₂Ni·4H₂O, 98.0%,

Sinopharm), cobalt acetate $((\text{CH}_3\text{COO})_2\text{Co}\cdot 4\text{H}_2\text{O}$, 99.5%, Sinopharm) and manganese acetate $((\text{CH}_3\text{COO})_2\text{Mn}\cdot 4\text{H}_2\text{O}$, 99.0%, Sinopharm) in ratio of 1.17:0.17:0.17:0.50 were used as raw materials of metal ions sources. The above mixtures were fully dissolved among ethanol ($\text{C}_2\text{H}_5\text{OH}$, 99.7%, Enox) by fast stirring in 40 °C for 0.5 h. After thoroughly dried in vacuum at 120 °C, the obtained acetate mixture was removed and ground totally for 0.5 h. The powdered pink acetate mixture was pre-annealed at 400 °C for 4 h and then followed by high-temperature calcination at 800 °C for 6 h in an atmosphere of air. After completely pestled in mortar, the final dark brown powder was carefully collected as the desired cathode material of Li-rich NCM.

Significantly, this Li-rich NCM cathode prepared via acetate precursor followed by two-step annealing process in air atmosphere could avoid the tedious and impure precursor treatment process for multi-transition metal hydroxides and complex compounds. The selected metal acetates here were all able to be dissolved fully among ethanol solvent, advantaging on dispersibility and uniformity for projected Li-rich NCM cathode and ultimately resulting in cathode with excellent electrochemical performance. This preparation route is easier and more efficient in upcoming commercialization of the layered-layered lithium rich cathode for Li-ion batteries.

The composite positive electrode was composed of 80 wt% Li-rich NCM active cathode, 10 wt% acetylene black (Super-P, conducting additive) and 10 wt% polyvinylidene fluoride (PVDF, binder). After mixed thoroughly and uniformly, the obtained slurry was firmly coated on the aluminum foil current collector by notch bar and entirely dried in vacuum at 100 °C. The round positive electrode laminates (diameter=14 mm) were punched for assembling CR2016-type coin cells in the argon-filled glove box. 1 M LiPF_6 dissolved in the solvent mixture (1:1, vol%) of ethylene carbonate (EC) and dimethyl-carbonate (DMC) was employed as the electrolyte and Celgard 2300 membrane was applied as separator. The Li metal foil was adopted to be negative electrode and reference electrode as well. Li-rich NCM/Li coin cells were tested by multi-channel battery test system (CT2001A cell test instrument, LAND Electronic Co.) under galvanostatically charging and discharging at different C rates (nominal capacity=200 mAh g^{-1} , 1C=200 mA g^{-1}) within cutoff voltage limits between 2.0 V to 4.8V at room temperature.

X-ray diffraction (XRD, Cu $\text{K}\alpha$ radiation, Bruker, D8 Advance, Germany) was used to characterize the crystalline structure over 2θ range from 10° to 70°. The morphology of prepared Li-rich NCM cathode powder was illustrated by Scanning Electron Microscopy (SEM, SU-1500, HITACHI, Japan).

Electrochemical Impedance Spectroscopy (EIS) was implemented over the frequency range of 0.01 Hz to 100 kHz with the perturbation AC voltage signal of 5 mV. The Zview fitting software was selected to simulate the measured results to further detail electrochemical dynamic parameters. The fresh cells were charged and discharged for at least 2 cycles previously in order to activate and stabilize the internal electrochemical system. Cyclic voltammetry (CV) was implemented at a scan rate of 10 $\mu\text{V s}^{-1}$ in the potential range from 2.5 V to 4.8 V to reflect the intercalation/deintercalation kinetics. All these electrochemical tests were executed by CHI660C workstation (CHENHUA Instrument, China).

3. RESULTS AND DISCUSSION

3.1. Structure and morphology

Fig. 1 shows the XRD pattern of Li-rich NCM cathode powder sample. Most peaks indicate a typical α -NaFeO₂ layered hexagonal structure that belongs to space group of $R\bar{3}m$ except for the super-lattice peaks present between 20° and 25°. These weak reflections near 21° are considered as the feature of the complex Li[Li_{1/3}Mn_{2/3}]O₂-LiMO₂, corresponding to the in-plane Li/Mn ordering in transition metal layers originated from monoclinic Li[Li_{1/3}Mn_{2/3}]O₂-like super lattice (C2/m) [24-28]. The XRD spectrum of Li-rich NCM powder clearly shows the splitting of (006)/(102) and (108)/(110) doublets [22], implying that the powder sample has a well-organized layered structure. Along with the integrated intensity ratio of (003) and (104) peaks $I_{(003)}/I_{(104)}$ obviously higher than 1.2 (which equals to 1.88 here), this XRD pattern reveals an extremely high crystallinity of the prepared Li-rich NCM [24,25].

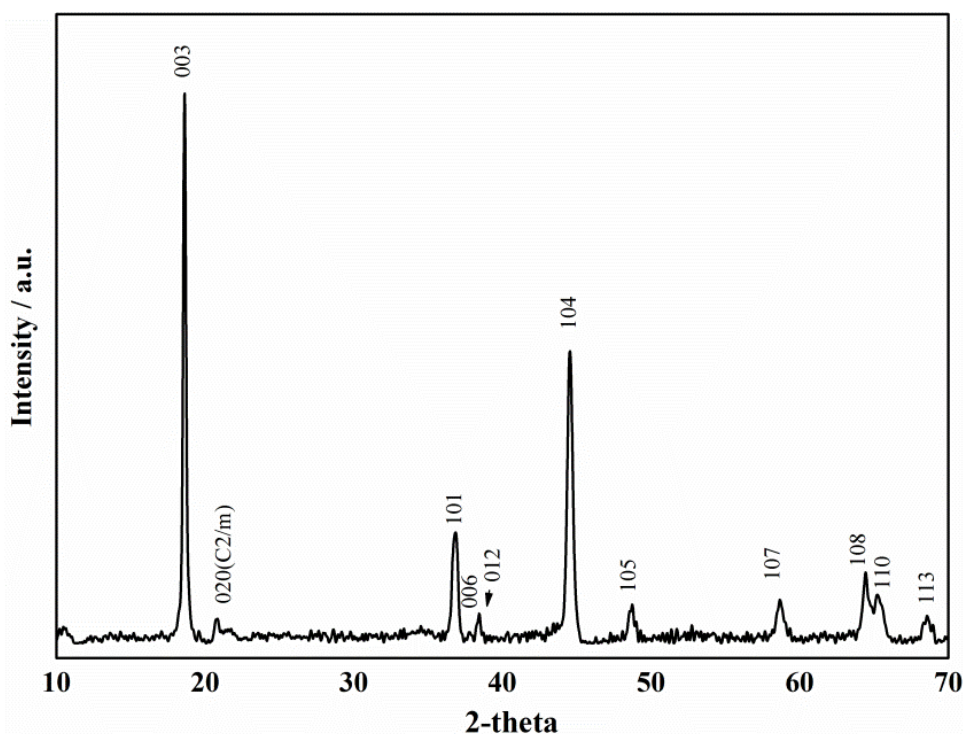


Figure 1. XRD pattern of prepared Li-rich NCM cathode powder.

The morphology of the Li-rich NCM powder particles, investigated by scanning electron microscopy (SEM), is shown in Fig.2. The SEM images distinctly illustrate that this Li-rich NCM powder contains little and tiny aggregates, which is consisted of homogeneous and round-sharp primary particles with small size distribution between 70 and 280 nm (observed apparently in Fig.2d). Since smaller particles implying shorter Li-ion diffusion path during the cycling process [26,28], the intercalation and de-intercalation of Li-ion internal this Li-rich NCM cathode could be much faster, thus finally initiating better charge and discharge properties especially at high C-rate cycling.

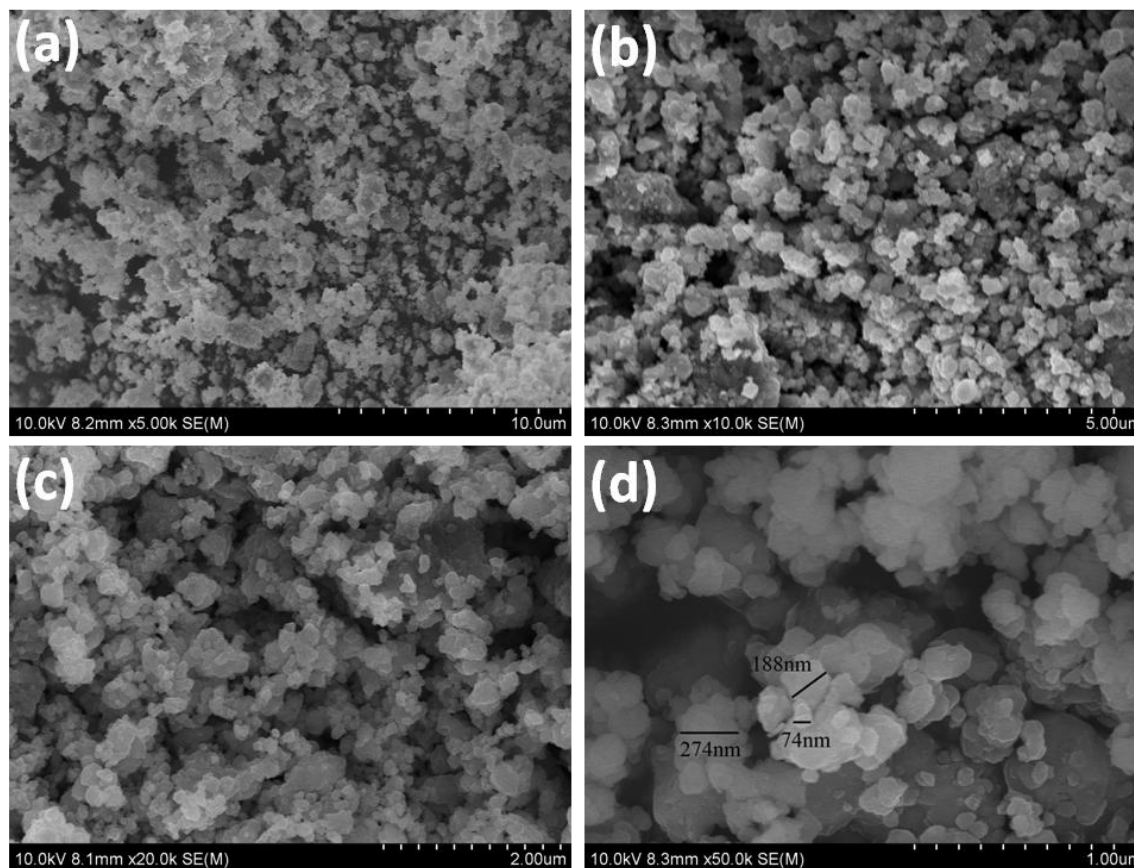


Figure 2. SEM pictures of Li-rich NCM particles at (a) $\times 5k$, (b) $\times 10k$, (c) $\times 20k$, and (d) $\times 50k$ magnification.

3.2. Charge and discharge performance

Fig. 3(a) compares the initial charge-discharge profiles of the prepared Li-rich NCM composite electrodes at different C-rates within cutoff voltage ranges of 2.0 V to 4.8 V. As stated in XRD characterization, the Li-rich NCM composite electrodes exhibits two distinguishable voltage plateaus during the first charge due to the existence of different lithium de-intercalation processes in layered hexagonal and monoclinic structure. The first plateau is located from 3.7 V to 4.5 V where the delivered capacity is associated to the oxidation process of $Ni^{2+} \rightarrow Ni^{4+}$ and $Co^{3+} \rightarrow Co^{4+}$ during the lithium de-intercalation among $Li[Ni_{1/3}Co_{1/3}Mn_{1/3}]O_2$ -like region [12,26-28]. In this plateau, all electrodes deliver almost the same capacity (about 100-130 $mAh\ g^{-1}$) at varied C-rates. The electrodes then show a long and smooth plateau located above 4.5 V, corresponding to the simultaneous removal of Li^+ and O^{2-} in formation of Li_2O from the layered $Li[Li_{1/3}Mn_{2/3}]O_2$ lattice to be transformed into a MnO_2 -like phase [8,11,28]. The capacity delivered in second plateau decreases strongly (130.4 $mAh\ g^{-1}$ at 0.2C and 60.5 $mAh\ g^{-1}$ at 5C) when C-rate increases, indicating rather slower kinetics during this process. It is observed from Fig.3 that the electrodes deliver initial discharge capacities of 218.2 $mAh\ g^{-1}$, 199.3 $mAh\ g^{-1}$, 177.5 $mAh\ g^{-1}$, 161.5 $mAh\ g^{-1}$ and 131.6 $mAh\ g^{-1}$ at 0.2C, 0.5C, 1C, 2C, and 5C, respectively. The excellent electrochemical performance of the as-prepared Li-rich NCM cathode could

be expected because of well-projected layered structure reflected by XRD pattern and favorable primary particles morphology of little aggregates and small size distributions demonstrated by SEM images.

Table 1. Capacity delivered of the Li-rich NCM composite electrodes at different C-rates

| No. | Discharge capacity (mAh g ⁻¹) | | | | |
|-------------------|-------------------------------------------|-------|-------|-------|-------|
| | 0.2C | 0.5C | 1C | 2C | 5C |
| 1 st | 218.2 | 199.3 | 177.5 | 161.5 | 131.6 |
| 30 th | 200.6 | 193.1 | 169.3 | 146.5 | 115.4 |
| 50 th | 200.6 | 191.2 | 161.3 | 142.3 | 111.7 |
| 80 th | 192.4 | 178.9 | 152.2 | 141.4 | 112.0 |
| 100 th | 185.5 | 171.6 | 151.1 | 141.9 | 112.7 |

Cycling performance is one of the most important electrochemical characteristics for Li-ion batteries.

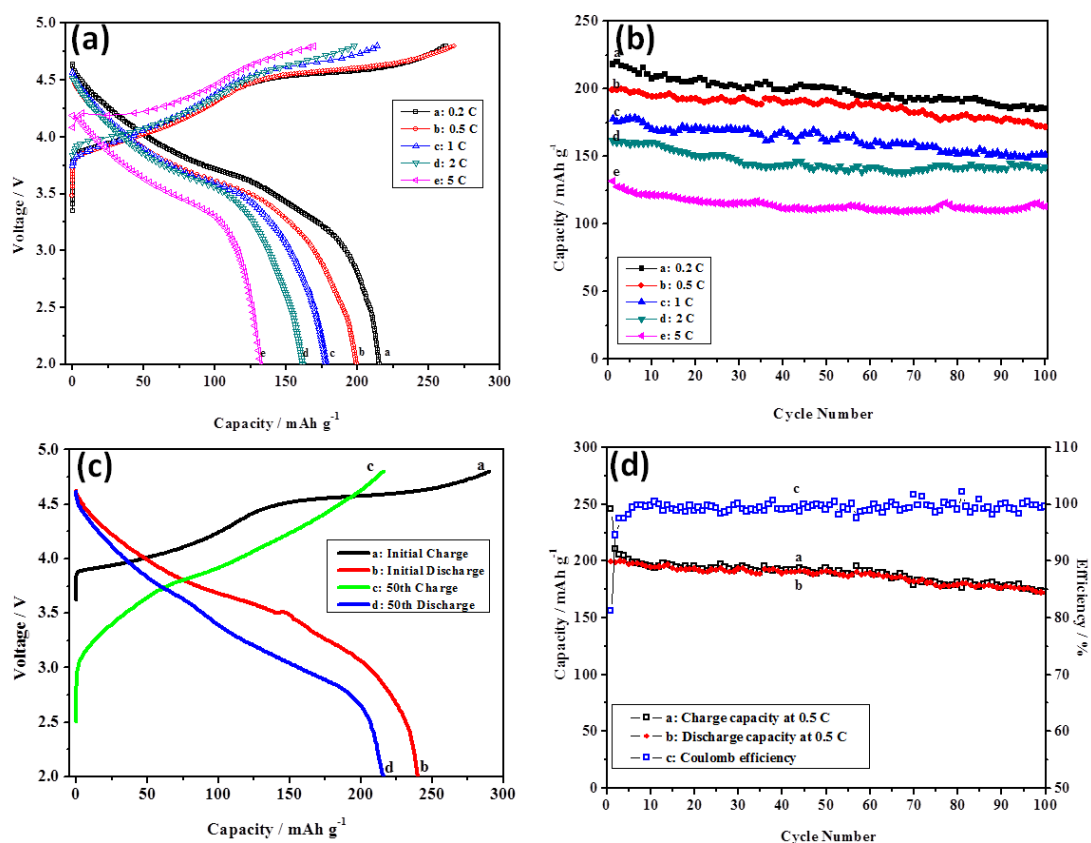


Figure 3. (a) Initial charge-discharge curves of Li-rich NCM composite electrodes at different C-rates; (b) Cycling behaviors at various discharge C-rates of the Li-rich NCM composite electrodes; (c) The initial and 50th charge-discharge curves of Li-rich NCM composite electrode at 0.1C; (d) Charge-discharge performance and coulomb efficiency of the Li-rich NCM composite electrodes at 0.5C.

Fig. 3(b) shows the cycling behaviors of the Li-rich NCM composite electrodes at various discharge C-rates within the cutoff voltage limits between 2.0 V and 4.8 V at room temperature. Although all curves in this Fig. 3(b) are slightly undulated, the general trend during cycling is gradually declined as a result of Li-rich NCM active mass dissolution in the electrolyte or any other side reactions within continuous cycling process. These capacity fades are in good agreement with electrochemical testing results of EIS and CV data. The delivered capacities at 1st, 30th, 50th, 80th, and 100th cycles are also listed in Table 1. Remarkably, very slow discharge capacity loss after cycled for 30 times especially at high C-rates and discharge capacity retention over 85.0% at each C-rate after 100 cycles that take place (Table 1).

Fig.3(c) illustrates the initial and 50th charge-discharge performance of Li-rich NCM composite electrode within cutoff voltage ranges of 2.0 V to 4.8 V at 0.1C. The initial charge and discharge capacities of this Li-rich NCM composite electrode are 293.2 mAh g⁻¹ and 240.1 mAh g⁻¹ at 0.1C, respectively. The reversible capacity retention is about 89.9% after 50 cycles under this C-rate condition, as shown in the Fig.3(c). The irreversible capacity loss of the "layered-layered" xLi[Li_{1/3}Mn_{2/3}]O₂·(1-x)LiMO₂ as large as 50 to 100 mAh g⁻¹ during first cycle could be ascribed to the side products generation of electrolyte oxidation reactions or the structural and phase transitions caused by oxygen vacancies elimination when the Li⁺ is extracted in Li₂O formation during the electrochemical activation of Li[Li_{1/3}Mn_{2/3}]O₂ as reported in recent literatures [7-9,26-28]. Fig.3(d) reveals charge-discharge performance and its coulomb efficiency of the prepared Li-rich NCM composite electrode at 0.5C, where a steady and high discharge capacity has been delivered with retention above 86.0 % after 100 cycles.

3.3. Cyclic voltammetry

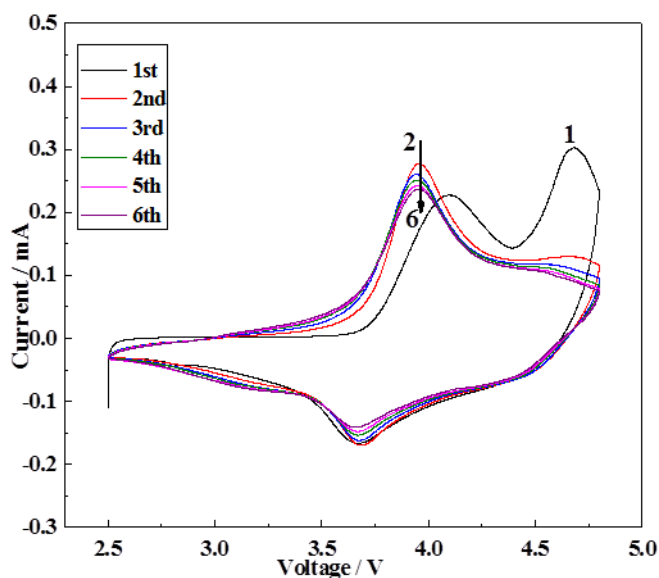


Figure 4. Cyclic voltammograms of Li-rich NCM composite electrode at a scanning rate of 100 $\mu\text{V s}^{-1}$ between the potential cutoff ranges of 2.5 V to 4.8 V.

Cyclic voltammetry (CV) has been performed to understand the kinetic behaviors of Li-rich NCM composite electrodes. The data is carried out at a scanning rate of $100 \mu\text{V s}^{-1}$ over the potential from 2.5 V to 4.8 V at room temperature for 6 cycles. Fig.4 exhibits typical initial and following 5 cyclic voltammograms. As we can see from the Fig.4, the first CV curve shows a large anodic peak after 4.4 V differing from any other overlapped cycles, implying the occurrence of irreversible monoclinic phase transition. The large irreversible capacity during its initial cycling is aptly reflected in initial cyclic voltammogram. The subsequent successive CVs are well overlapped although current intensity is slowly declined, resulting in gradually but slightly capacity fades.

In order to obtain further kinetic information of the Li-rich NCM composite electrode, we have calculated the diffusion coefficient of lithium ions (D_{Li}) according to the peak current $I_p(A)$ and the square root of scanning rate $v^{1/2} (\text{V}^{1/2} \text{s}^{-1/2})$ by the following equation [29,30]:

$$I_p = 2.69 \times 10^5 n^{3/2} A D_{Li}^{1/2} C v^{1/2};$$

Where n refers to the electron number per reaction species, A is the electrode surface area (1.54 cm^2 here) and C is the bulk concentration of lithium ions in electrode. The calculated lithium ion diffusion coefficient D_{Li} is $1.39 \times 10^{-11} \text{ cm}^2 \text{ s}^{-1}$.

3.4. Electrochemical Impedance Spectroscopy

Electrochemical impedance spectroscopy (EIS) is another powerful electrochemical tool to identify kinetic parameters of lithium intercalation/de-intercalation into electrode.

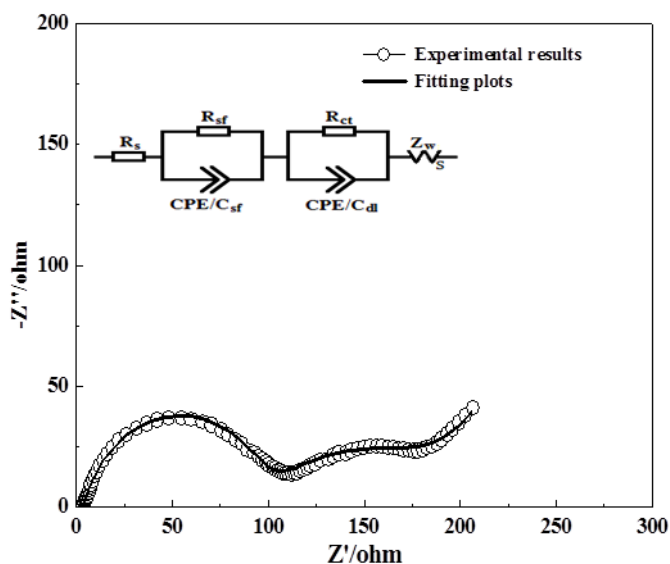


Figure 5. The Nyquist plots of the Li-rich NCM composite electrode after charged to 4.8 V; experimental results vs. fitting plots and the equivalent circuit model (inset in Fig.5).

EIS has been carried out to investigate the electrochemical parameters of this Li-rich NCM composite electrode in this paper. All possible and experimentally observed electrochemical processes

may include [22-26]: (1) a resistive component R_s coming from the electrolyte resistance and cell components; (2) the surface film resistance R_{sf} and its capacitance C_{sf} including the resistance and capacitance of solid electrolyte interface (SEI); (3) the charge transfer resistance R_{ct} and related double-layer capacitance C_{dl} ; and (4) the Warburg impedance Z_w to solid-state diffusion of lithium ions through the bulk of active material. The electrode kinetics is controlled by the charge transfer contribution [31-34].

Fig.5 presents the experimental Nyquist plots of the Li-rich NCM composite electrode and its fitting results after fully charged to 4.8 V. The plots show two overlapped semicircles and a straight sloping line. The high frequency semicircle indicates the impedance R_{sf} and C_{sf} due to SEI film formed on the Li-rich NCM composite electrode surface. The intermediate frequency semicircle is interrelated to charge transfer resistance R_{ct} in electrode/electrolyte interface and associative double layer capacitance C_{dl} . A straight line in the low frequency region is influenced by Warburg impedance Z_w arising from the lithium ions diffusion internal electrode. The equivalent circuit model shown in inset adopted to simulate the experimental Nyquist plots by fitting software Zview. The most important electrochemical parameter R_{ct} , which is attributed to the charge transfer process in electrode/electrolyte interface, is calculated by the Zview. The results in Fig.8 show that R_{ct} of this Li-rich NCM cathode electrode is as lower as 72.11 Ω , confirming by the excellent electrochemical performance of prepared Li-rich NCM cathode.

4. CONCLUSIONS

Li-rich "layered-layered" cathode $\text{Li}_{1.17}[\text{Ni}_{0.17}\text{Co}_{0.17}\text{Mn}_{0.50}]\text{O}_2$ has been successfully synthesized using acetate precursor by solid state method in this paper. XRD results show a well layered-structure mainly belonging to of $R-3m$ space group except for little super-lattice originating from the monoclinic $\text{Li}[\text{Li}_{1/3}\text{Mn}_{2/3}]\text{O}_2$ -like phase. SEM pictures present narrow primary particle size distribution (70 nm to 280 nm). The small and homogeneous primary particles are very helpful to improve the electrochemical properties and charge-discharge performance of the prepared Li-rich NCM cathode. The composite electrode could deliver an initial reversible capacity as high as 240.1 mAh g^{-1} at 0.1C and remarkable reversible capacity retention after 100 cycles could be achieved especially at high C-rates. The lithium ion diffusion coefficient D_{Li} is calculated to be $1.39 \times 10^{-11} \text{ cm}^2 \text{ s}^{-1}$ while the charge transfer resistance R_{ct} is as lower as 72.11 Ω , which is fitted and simulated by Zview.

The highlight of this Li-rich NCM cathode material is the excellent electrochemical performance along with convenient preparation adopting acetate precursor by solid state method. Integrated the feasible and accessible treatment on acetate precursor with economic solid state method preparation, these Li-rich NCM cathodes may fulfill the requirements of high performance and low cost for lithium ion batteries on usage of hybrid-electric vehicles and other high energy power devices. However, this Li-rich NCM cathode still suffers some drawbacks like rapid initial capacity fading. The improvement works by appropriate surface modification will be reported in the future.

ACKNOWLEDGEMENTS

This work was supported by Shanghai Natural Science Fund (No.15ZR1418100) and Shanghai Enterprise Independent Innovation Special Project (No.CXY-2014-24) and Shanghai Science and Technology Committee (No. 14DZ2261000).

References

1. H. Yu and H. Zhou, *J Phys Chem Lett*, 4 (2013) 1268.
2. Y. Zhou, J. Ma, E. Hu, X. Yu, L. Gu, K. W. Nam, L. Chen, Z. Wang and X. Q. Yang, *Nature communications*, 5 (2014) 5381.
3. E. McCalla, A. S. Prakash, E. Berg, M. Saubanere, A. M. Abakumov, D. Foix, B. Klobes, M. T. Sougrati, G. Rousse, F. Lepoivre, S. Mariyappan, M. L. Doublet, D. Gonbeau, P. Novak, G. Van Tendeloo, R. P. Hermann and J. M. Tarascon, *J. Electrochem. Soc.*, 162 (2015) A1341.
4. X.Zhang, W. Jiang, A. Mauger, Qilu, F. Gendron, C.M. Julien, *J. Power Sources*, 195 (2010) 1292.
5. M. Lengyel, G. Atlas, D. Elhassid, X. Zhang, I. Belharouak and R. L. Axelbaum, *J. Electrochem. Soc.*, 161 (2014) A1023.
6. X. Yuan, Q.Xu, C. Wang, X. Liu, H. Liu and Y. Xia, *J. Power Sources*, 279 (2015) 157.
7. M.M. Thackeray, S.H. Kang, C.S. Johnson, J.T. Vaughey, R. Benedek, S.A. Hackney, *J. Mater. Chem.*, 17 (2007) 3112.
8. K.A. Jarvis, Z. Deng, L.F. Allard, A. Manthiram, P.J. Ferreira, *Chem. Mater.*, 23 (2011) 3614.
9. S.H. Park, S.H. Kang, C.S. Johnson, K. Amine, M.M. Thackeray, *Electrochem. Commun.*, 9 (2007) 262.
10. L. Boulet-Roblin, M. E. Kazzi, P. Novak and C. Villevieille, *J. Electrochem. Soc.*, 162 (2015) A1297.
11. X. Jin, Q. Xu, X. Yuan, L. Zhou and Y. Xia, *Electrochimica Acta*, 114 (2013) 605.
12. H. Koga, L. Croguennec, M. Menetrier, K. Douhil, S. Belin, L. Bourgeois, E. Suard, F. Weill, C. Delmas, *J. Electrochem. Soc.*, 160 (2013) A786.
13. X. Jin, Q. Xu, H. Liu, X. Yuan and Y. Xia, *Electrochimica Acta*, 136 (2014) 19.
14. L. Croguennec and M. R. Palacin, *J. Am. Chem. Soc.*, 137 (2015) 3140.
15. H. Iddir, B. Key, F. Dogan, J. T. Russell, B. R. Long, J. Bareño, J. R. Croy and R. Benedek, *J. Mater. Chem.A*, 3 (2015) 11471.
16. J. Liu, Q. Wang, B. Reeja-Jayan, A. Manthiram, *Electrochem. Commun.*, 12 (2010) 750.
17. J.M. Zheng, X.B. Wu, Y. Yang, *Electrochim.Acta.*, 56 (2011) 3071.
18. J. Liu, A. Manthiram, *J. Mater. Chem.*, 20 (2010) 3961.
19. Y.H. Xiang, Z. Yin, Y.H. Zhang, *Electrochim. Acta*, 91 (2013) 214.
20. T. Ohzuku, M. Nagayama, K. Tsuji, K. Ariyoshi, *J. Mater. Chem.*, 21 (2011) 10179.
21. J. Liu, B. Reeja-Jayan, A. Manthram, *J. Phys. Chem. C*, 114 (2010) 9528.
22. S.K. Martha, J. Nanda, G.M. Veith, N.J. Dudney, *J. Power Sources*, 199 (2012) 220.
23. L.Z. Zhou, Q.J. Xu, M. S. Liu, X. Jin, *Solid State Ionics*, 249 (2013) 134.
24. J. R. Croy, A. Abouimrane and Z. Zhang, *MRS Bulletin*, 39 (2014) 407.
25. A. Boulineau, L. Croguennec, C. Delmas, F. Weill, *Solid State Ionics*, 180 (2010) 1652.
26. J. Li, R. Klopsch, M.C. Stan, S. Nowak, M. Kunze, M. Winter, S. Passerini, *J. Power Sources*, 196 (2011) 4821.
27. J.S. Kim, C.S. Johnson, J.T. Vaughey, M.M. Thackeray, S.A. Hackney, *Chem. Mater.*, 16 (2004) 1996.
28. M. Tabuchi, M. Kitta, H. Kageyama, H. Shibuya and J. Imaizumi, *J. Power Sources*, 279 (2015) 510.
29. Y. Jin, C.P. Yang, X.H. Rui, T. Cheng, C.H. Chen, *J. Power Sources*, 196 (2011) 5623.

30. J. Zheng, M. Gu, A. Genc, J. Xiao, P. Xu, X. Chen, Z. Zhu, W. Zhao, L. Pullan, C. Wang and J. G. Zhang, *Nano letters*, 14 (2014) 2628.
31. A. Klein, P. Axmann, C. Yada and M. Wohlfahrt-Mehrens, *J. Power Sources*, 288 (2015) 302.
32. H.J. Kim, H.G. Jung, B. Scrosati, Y.K. Sun, *J. Power Sources*, 203 (2012) 115.
33. X. Wei, S. Zhang, L. He, G. Liu, P. Yang, *Int. J. Electrochem. Sci.*, 8(2013) 1885.
34. F. Feng, H. Fang, B. Yang, W. Ma, Y. Dai, *Int. J. Electrochem. Sci.*, 9 (2014) 6852.

© 2015 The Authors. Published by ESG (www.electrochemsci.org). This article is an open access article distributed under the terms and conditions of the Creative Commons Attribution license (<http://creativecommons.org/licenses/by/4.0/>).